Astron. Astrophys. 198, 16–32 (1988)

ASTRONOMY AND ASTROPHYSICS

III Zw 2: a look into the AGN machinery

J.S. Kaastra and P.A.J. de Korte

Laboratory for Space Research Leiden, Niels Bohrweg 2, P.O. Box 9504, NL-2300 RA Leiden, The Netherlands

Received August 17, accepted November 4, 1987

Summary. The radio to X-ray properties of the quasar III Zw 2 are investigated and the physical conditions in several parts of the nucleus are derived. The accretion disk has a large thickness in the central part (maximum relative thickness 0.8) and probably extends to 0.2 pc, thus hiding a certain part (30%) of the broad line region clouds. A very compact X-ray source (about 3 Schwarzschild radii) radiating near the Eddington limit is feeded by soft disk photons which are scattered by the inverse Compton effect up to X-ray energies. Due to the disk thickness the X-rays show a moderate degree of beaming. The accretion rate on the $5\,10^7\,M_\odot$ central black hole is that high that the accretion process cannot have lasted longer than 20 million years. Finally, observations of a rapid X-ray absorption feature in III Zw 2 are interpreted as photo-absorption due to a fast infalling ($\sim 0.5c$), hot (10^6 K) cloud near the innermost radius (10^{14} m) it can reach before being dissolved.

Key words: accretion disks – active galactic nuclei – quasars, X-rays – quasars, variations

1. Introduction

The X-ray spectrum of Seyfert galaxies and QSO's is known to be time variable. Since X-rays originate from regions close to the central powerhouse of an active galaxy, variations in the X-ray flux provide unique information about nuclear activity. Variations in amplitude by a factor two on time scales of a month to years have been observed (Marshall et al., 1981; Zamorani et al., 1984; Petre et al., 1984). The variations have an amplitude range of a factor 2 (Zamorani et al., 1984). Shorter lasting variations (less than 1000 s) have been reported recently for low luminosity (10^{34} W) Seyferts (Lawrence et al., 1985; Barr et al., 1985). Unlike BL Lac objects, Seyferts and QSO's show a marked correlation between their variation time constant and their 2–10 keV luminosity, ranging from 100 s at 10^{34} W to a few weeks at 10^{39} W (Barr and Mushotzky, 1986).

The longer time scale observed for high luminosity QSO's compared to less luminous objects is explained commonly by assuming that the more powerful X-ray sources have a larger mass and Schwarzschild radius, resulting in longer time constants due to light travel time arguments. Detection of much faster (~ 1 hour) fluctuations in the high luminosity objects would imply luminosities close to the Eddington limit. Such fast fluctuations have been reported definitely by Matilsky et al. (1982) for the quasar 1525 + 227, where variations of 10^{35} W s^{-1} seem to occur; however no spectral information was obtained. Rapid variations with spectral information in the AGN III Zw 2 were reported by Kaastra and de Korte (1986) and Pounds (1986). In the first paper a fast absorption feature is analysed while in the other a flare is reported.

In the present paper we investigate the properties of III Zw 2 which follow from these X-ray observations and from the observations at other frequencies, reported in the literature. The physical conditions near the central black hole, in the accretion disk, the broad line region and the synchrotron sources are deduced in some detail.

In Sect. 2.2 we discuss the optical/UV continuum data. These data contain important information on the accretion disk parameters. Next we consider the radio and infrared synchrotron source, which leads us to estimates of the magnetic field. In Sect. 2.4 the narrow and broad lines are investigated and the physical parameters in both regions are derived. The line profiles of the broad lines yield us the dynamical parameters of that region and the radius of the accretion disk. After summarizing previous X-ray observations in Sect. 2.5, we give a detailed account of new EXOSAT observations of III Zw 2 in Sect. 3. In Sect. 4 we combine our findings obtained from the different wavelength regions in order to study the accretion process in the quasar. We summarize in Sect. 5.

2. Physical properties of III Zw 2 derived from non X-ray wavelengths

2.1. Parent galaxy

III Zw 2 was discovered by and named after Zwicky (1964, 1969). It is classified either as a type 1 Seyfert galaxy (Arp, 1968; Khachikian and Weedman, 1974; Osterbrock, 1977) or as a quasar (Green et al., 1978). Assuming $H_0 = 50\,\mathrm{km\,s^{-1}\,Mpc^{-1}}$, $q_0 = 0.5$ as throughout this paper, the distance derived from its redshift $z = 0.0898$ (de Robertis, 1985) is 550 Mpc (luminosity distance) or 460 Mpc (angular size distance).

The parent galaxy is a spiral with a typical radius of 14 kpc (Hutchings et al., 1982). It has a strong, blue nucleus which is 40 times stronger than the whole galaxy in the *B*-band (Hutchings et al., 1984). The inclination derived from the apparent flattening of the blue isophotes (Hutchings et al., 1984) is 33°. The isophotes

Send offprint requests to: J.S. Kaastra

are somewhat rounder in the centre of the galaxy. There is an asymmetrical extension to the north of the galaxy, at P.A. 350° (Arp, 1968; Green et al., 1978). This may be due to interactions with other galaxies, for III Zw 2 is the brightest member of a cluster or group of galaxies; a companion galaxy at 110 kpc distance is found south of it (Sargent, 1970; Green et al., 1978; Heckman et al., 1984). The neutral hydrogen mass derived from the 21 cm line (Hutchings et al., 1987) is $5\,10^{10}\,M_{\odot}$.

The source is variable in all wavelength regions from radio to X-rays; in the optical (Green, 1976; Pica et al., 1980; Lloyd, 1984), infrared (Rieke and Lebofsky, 1979; Lebofsky and Rieke, 1980; Neugebauer et al., 1986) and ultraviolet region (Huchra et al., 1981; Chapman et al., 1985) variations of a factor 2 in a few months occur.

2.2. *Accretion disk*

Figure 1 shows the optical and radio intensity time profile of III Zw 2. Although the optical data suffer from the selection effect that no observations have been made in the first half of the year, it is clear from Fig. 1 that III Zw 2 shows several flare-like features with a frequency of one each 1–2 years. The minimum flux level in the *B*-band is about 1 mJy, corresponding to $B \simeq 16.2$. The flux at the end of 1978 was at least 4.5 times stronger than this minimum level. We estimated the exponential decay times of the flares at September 1971, September 1974, October 1975 and September 1976 (Table 1); the mean decay time was 12.5 ± 1.4 month, with individual values ranging from 11–15 month. Subtracting first a "steady" flux level of ~1 mJy does not change these numbers significantly. The exponential rise time of the only flare for which we could determine it, at November 1978, was somewhat shorter than the average decay time, 7.8 ± 1.5 month. If this flare has a similar decay time as the other flares, the total energy output in the *B*-band of this flare is $1.0\,10^{31}\,\mathrm{J\,Hz^{-1}}$. The effective bandwidth of the optical flare is about 10^{15} Hz (Fig. 2) hence a total amount of 10^{46} J is converted in the flare.

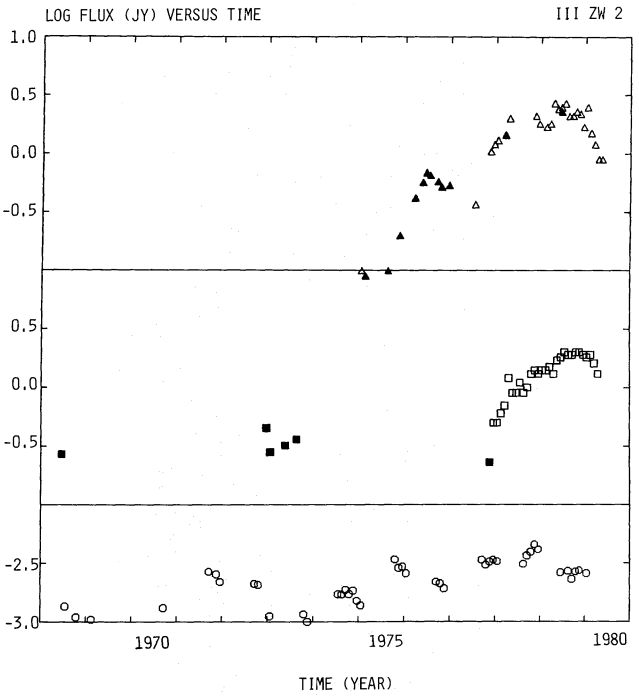

Fig. 1. Time history of the outbursts in III Zw 2. Monthly averages are shown. The flux scale is logarithmic, units: Jansky. Lower panel, open circles: optical *B*-band flux, taken from Pica et al. (1980) and Lloyd (1984). Second panel, filled squares: 2.7 GHz, from Huchtmeier and Wright (1973) and Kojoian et al. (1977); open squares: 8 GHz, from Aller et al. (1981). Upper panel, filled triangles: ~10.7 GHz, from Andrew et al. (1978), Wittels et al. (1978), and Balonek et al. (1979); open triangles: ~14.5 GHz, from Wright et al. (1977), Schnopper et al. (1978), and Aller et al. (1981)

Table 1. Rise times (t_r) and decay times (t_d) of the optical flares in III Zw 2

Time of maximum (mon. yr)	t_r (10^7 s)	t_d (10^7 s)
9. 1971	–	3.9 ± 1.8
9. 1974	–	3.5 ± 0.5
10. 1975	–	2.9 ± 0.6
9. 1976	–	4.1 ± 2.1
11. 1978	2.1 ± 0.4	–

The spectral energy distribution of III Zw 2 is shown in Fig. 2. As commonly found in quasars, the energy distribution between 10^{12} and 10^{18} Hz is constant within a factor of 4; caution should be taken however, because the XUV spectrum is unknown, and because the source is variable with a similar amplitude.

The increase of the energy density in the optical part of the spectrum, near 10^{15} Hz, can be interpreted as due to blackbody radiation from an accretion disk (Shields, 1978; Malkan and Sargent, 1982). The spectrum of such a disk, if the disk is thin, can be calculated from the temperature distribution at the surface as given by Shakura and Sunyaev (1973):

$$T_s = (3\,GM\dot{M}/8\pi\sigma r^3)^{1/4} \tag{1}$$

leading to

$$L_\nu = 4.1607[(GM\dot{M})^2 h\nu/c^2]^{1/3} f(\nu), \tag{2}$$

with

$$f(\nu) = 0.5176 \int_{h\nu/kT_m}^{\infty} x^{5/3}/(e^x - 1)\,dx \tag{3}$$

where M is the mass of the central object, $\dot{M}$ the accretion rate onto the central object, r the radial distance, ν the frequency and σ is the constant of Stefan-Boltzmann. T_m is the maximum temperature of the disk, reached at its innermost radius. The function f equals 1 for small values of the frequency, resulting in a $\nu^{1/3}$ spectrum at low frequencies.

We fitted the optical spectrum of III Zw 2 at the three dates indicated in Fig. 2 with the spectrum (3). The extrapolation of the infrared power law continuum, which contributes to about half of the optical flux, was subtracted first using the observed H-L color index. The resulting disk luminosities are in the range $6\text{–}11\,10^{22}\,\mathrm{W\,Hz^{-1}}$ at 10^{15} Hz, while the average of the maximum temperature T_m is 35000 K (Table 2).

This is compatible with the average temperature derived for a large sample of quasars, which was 26000 K with a standard deviation of 4000 K (Edelson and Malkan, 1986). Edelson and Malkan fitted a simple one-temperature component, instead of a

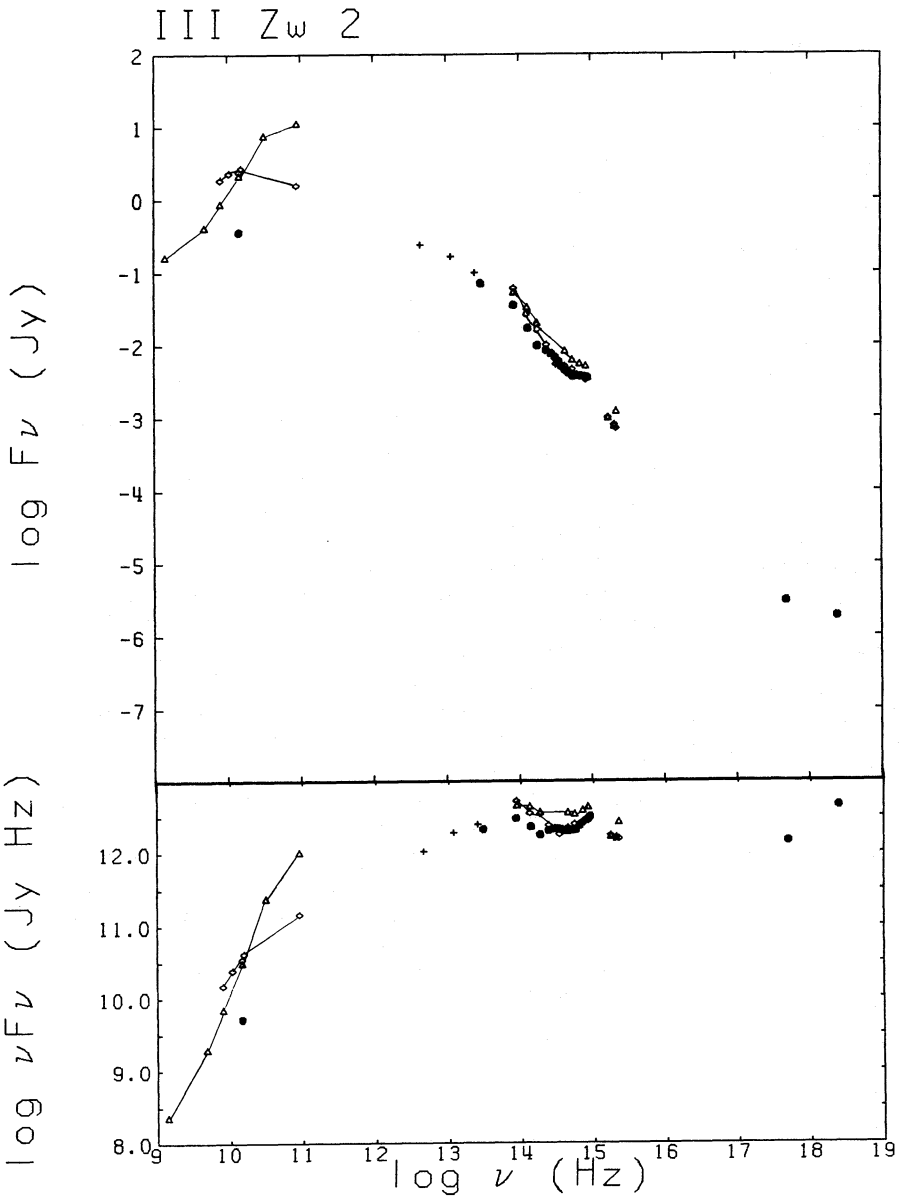

Fig. 2. Spectral energy distribution in III Zw 2 at three dates. Upper panel: flux versus frequency; lower panel: flux times frequency versus frequency. The continuous lines are only drawn to guide the eye. Filled circles: July 1977 (Wright et al., 1977; Neugebauer et al., 1979; Schnopper et al., 1978) Open triangles: June 1978 (Condon et al., 1981; Chapman et al., 1985); the radio part of the spectrum consists of the January 1978 spectrum (Schnopper et al., 1978) scaled to the June 1978 spectrum using the 8.0 GHz flux from Aller et al. (1981) which is known at both times. Open diamonds: August 1979 (Aller et al., 1981; Balonek and Dent, 1979 (June 1979, scaled to August using Aller et al. 1981); Landau et al. (July 1979, scaled as above); McAlary et al., 1983; Chapman et al., 1985). Crosses: IRAS data (Neugebauer et al., 1986)

Table 2. Accretion disk parameters derived from 3 spectra

	Date		
	7.1977	6.1978	8.1979
Infrared power law energy index	1.70	1.30	1.56
Infrared power law luminosity at 10^{15} Hz (10^{22} W/Hz)	2.1	8.8	5.2
Disk luminosity at 10^{15} Hz (10^{22} W/Hz)	10.6	8.3	5.8
T_m (K)	–	33000 ± 7000	36000 ± 4000
$M\dot{M}$ ($10^8 M_\odot^2\,yr^{-1}$)	1.8	1.2	0.7
Total disk luminosity (10^{38} W)		1.0	1.0

disk spectrum; if we fit our data with such a single temperature blackbody, the fitted temperature is about half T_m. The total optical-UV disk luminosity is of order 10^{38} W, comparable to the X-ray luminosity of the source. Using Eq. (2), it is possible to determine the product $M\dot{M}$. We find a weighted average value of $(1.1 \pm 0.4)\,10^8\,M_\odot^2\,\mathrm{yr}^{-1}$ for the three dates.

2.3. *Synchrotron source*

The strong radio flux from III Zw 2 classifies it as a radio-loud quasar; such quasars appear to have rather hard X-ray spectra, with hard X-ray photon indices typically of order 1.5, compared to radio quiet quasars with index 2 (Elvis et al., 1986). III Zw 2 forms no exception to this rule, as we will see in Sect. 3.

The radio spectrum has the typical slope of a self-absorbed synchrotron emitter up to at least 90 GHz (Schnopper et al., 1978; Fig. 2). But the spectrum is very variable; from 1975 to 1977 the radio flux increased by a factor of 10 (Wright et al., 1977). Smaller amplitude variations on the scale of a few months and even 13% flux changes in one day (Huchtmeier and Wright, 1973) indicate the presence of a very compact central source. The spectrum is nearly unpolarised (Aller et al., 1981; Rudnick et al., 1985).

VLBI observations (Schillizzi, 1976; Wittels et al., 1978; Lawrence et al., 1985; de Waard, 1986) show a compact central source containing some 80% of the total radio flux, and a more extended component (typical radius $2–3\,10^{17}$ m) which was identified as a jet-like extension at PA 148° (de Waard, 1986). The central core had a radius smaller than $1.4\,10^{16}$ m at 10.6 GHz in March 1978 (Wittels et al., 1978), it was smaller than $3\,10^{16}$ m at 5 GHz in June 1983 (de Waard, 1986), and smaller than $5\,10^{15}$ m at 22.3 GHz in January 1984 (Lawrence et al., 1985). Recently, VLA observations have shown the presence of a weak component at a distance of 10^{21} m from the core at PA 240° (Unger et al., 1987).

The time variability of the radio source (Fig. 1) may lead to an independent estimate of its size. The 14.5 GHz flux is strongly correlated with the 8 GHz flux; we found that the 8 GHz flux is delayed with respect to the 14.5 GHz flux by 4 ± 1 month. If we extrapolate this delay to 5 GHz, we expect a delay of about 7 month at 5 GHz. This delay is consistent with the times of maximum of the 1979 flare: about June 1979 (14.5 GHz, Fig. 1) and January 1980 (5 GHz, de Waard, 1986 and reference therein). The delays can be translated into a typical exponential frequency scale height of $5\,10^{15}$ m at 10.7 GHz.

Two large outbursts are evident from Fig. 1, one around 1972 and the other from 1975–1980.

The fast electrons causing the synchrotron emission are relativistic; if we assume that the fastest rise time of the outbursts (Table 3) corresponds to the light travel time through the emitting region, an exponential size at 10.7 GHz of $3.3\,10^{15}$ m is found. This size is comparable to the frequency scale height obtained before and consistent with the upper limit derived from the direct VLBI observations at the same time. If we identify the optical maximum at November 1978 with the radio maximum at August 1979, and if we assume that the radio source is powered by the central source, which is feeded by the accretion events corresponding to the optical outbursts, the delay implies a maximum distance of the radio source to the central powerhouse of $7\,10^{15}$ m. Such a delay of about 9 months is consistent with the characteristics of the 1972 flare and 1975/76 outburst.

Table 3. Rise times (t_r) and decay times (t_d) of the radio outbursts in III Zw 2

Start (mon. yr)	End (mon. yr)	t_r (10^7 s)	t_d (10^7 s)
4. 1975	2. 1976	1.4 ± 0.1	–
2. 1976	5. 1977	–	6.9 ± 0.8
5. 1977	10. 1977	1.1 ± 0.1	–
10. 1977	5. 1979	6.8 ± 0.5	–
8. 1979	3. 1980	–	1.7 ± 0.3

The magnetic field in the radio source can be derived using the turn-over frequency ν_m (the frequency where the self-absorbed synchrotron spectrum reaches its maximum flux S_m). Re-arrangement of the formula given by Kellerman and Pauliny-Toth (1969) yields:

$$B = 6.8\,10^6(\nu_m/T_{bm}^2)\cdot(1+z) \tag{4}$$

where the brightness temperature T_{bm} is given by:

$$kT_{bm} = \frac{S_m}{2\pi}(cd_A/r\nu_m)^2\cdot(1+z) \tag{5}$$

All quantities in Eq. (4) are in SI units (i.e. B in T, ν_m in Hz, T_{bm} in K). Further, r is the radius of the radio source, d_A the angular size distance and z the redshift.

The spectral turnover of the radio spectrum at August 1979 (Fig. 2) was somewhere between 14.5 and 90 GHz; at June 1978 however, it was larger than 90 GHz, although probably not much larger, because we see a flattening in the spectrum at 90 GHz. Therefore we insert $\nu_m = 10^{11.15\pm0.10}$ Hz, $S_m = 10^{1.0\pm0.1}$ Jy. The typical size at 10.7 GHz was $3.3\,10^{15}$ m, but at ν_m it is probably smaller. If we assume an exponential dependence of the frequency on the size we obtain a radius at ν_m of $1.3\,10^{15}$ m. As a characteristic value we adopt $\log r_m = 15.3 \pm 0.2$. We obtain a brightness temperature $10^{11.46\pm0.33}$ K and a typical magnetic field of $10^{-4.9\pm0.5}$ T. The estimate of B depends on the maximum frequency to the fifth power and on the radius of the source to the fourth power. The uncertainties in both quantities lead to the uncertainty of a factor of 3 in B. The brightness temperature of $3\,10^{11}$ K is close to the maximum value attainable before Compton scattering distorts the synchrotron spectrum (Kellerman and Pauliny-Toth, 1969). The ratio of the total synchrotron to Compton emissivity is proportional to the ratio of the magnetic energy density to the photon energy density (e.g., Rybicky and Lightman, 1979). Estimating the total received power at earth by $S_m\nu_m(1+z)$, we obtain for this ratio using (4):

$$U_{magn}/U_{ph} = 5.7\,10^{66}(1+z)^2/\nu_m T_m^5 \tag{6}$$

which is $10^{-1.6\pm0.7}$ in the present case.

Because of a lack in the present data between 10^{11} and 10^{13} Hz, it is not well possible to decide whether the infrared continuum matches the radio continuum. The infrared continuum (Fig. 2) probably has a turnover at $10^{12.5\pm0.5}$ Hz with a flux of $10^{-0.5\pm0.2}$ Jy. We insert these numbers in (4)–(6) and assume that the source radiates near its maximum brightness temperature (Edelson and Malkan, 1986). If we take the same value for U_{magn}/U_{ph} as for the radio source ($10^{-1.6\pm0.7}$) we obtain a brightness temperature of $10^{11.2\pm0.2}$ K, a magnetic field of $10^{-3\pm0.7}$ T and a radius of $10^{13.3\pm0.5}$ m.

Table 4. Spectral lines in III Zw 2

Element	Line	λ_0	f_{abs}	L (10^{35} W)	FWHM (km s^{-1})	References
H	Ly α	1216	1.59	98	4300	1, 2
	Hα	6563	1.12	62	4100	3, 4, 5, 6
	Hβ	4861	1.19	19	5200	3, 4, 5, 6, 7
	Hγ	4340	1.22	6.7	4200	3, 5, 6, 7
	Hδ	4102	1.23	1.4	2800	6, 7
	Pα	18751	1.04	4.6		4
He	He I	5876	1.14	2.7		4, 5, 6
	He II	4686	1.20	1.4		5
C	C III]	1909	1.64	16		1
	C IV	1549	1.50	68	4300	1, 2
N	[N II]	6583	1.12	0.84		5
	[N II]	6548	1.12	0.27		5
O	[O I]	6300	1.13	0.36		5
	O I	1304	1.60	3.8		2
	[O II]	3727	1.25	0.70	960	5, 7
	[O III]	5007	1.18	5.6	600	3, 4, 5, 6, 7
	[O III]	4959	1.18	1.9	670	5, 7
	[O III]	4363	1.22	0.19		5
Ne	[Ne III]	3869	1.25	1.9	1210	7
S	[S II]	6731	1.12	0.49		5
	[S II]	6716	1.12	0.49		5
Fe	Fe II	5320	1.16	2.0		5
	Fe II	5190	1.14	1.9		5
	Fe II	4570	1.20	4.3		5
	[Fe VII]	6087	1.14	<0.08		5
Mg	Mg II	2798	1.33	14		1

References: 1) Wu et al. (1983), 2) Chapman et al. (1985), 3) Neugebauer et al. (1979), 4) Puetter et al. (1981), 5) Osterbrock (1977), 6) de Bruyn and Sargent (1978), 7) Wilkes (1986)

2.4. Optical lines

2.4.1. The data available

Table 4 summarises the data on the optical lines identified in III Zw 2. The first column gives the name of the element, the second the name of the line or the ionisation stage, the third the rest wavelength of the line. We applied the reddening curve of Seaton (1979) in order to correct the data for galactic extinction. If we use a total neutral hydrogen density towards III Zw 2 of $4\,10^{24}$ m^{-2} (Heiles, 1975) and if we use the conversion of hydrogen density to visual absorption as given by Gorenstein (1975), we obtain a colour excess $E_{B-V} = 0.056$. The resulting reddening correction factor is listed in column 4. The total luminosity and the FWHM (full width at half maximum) are given in column 5 and 6. Both values are given in the restframe of III Zw 2. If more values were present, these values were averaged. The last column contains the references to the data.

2.4.2. Narrow line region

The density and temperature of the *narrow line* clouds can be estimated from the forbidden lines.

The ionisation parameter U is defined by

$$U = Q(H)/4\pi r^2 n_e c \qquad (7)$$

where $Q(H)$ is the number of ionising photons per second emitted by the central source, r the distance of the cloud to the central source and n_e the electron density of the cloud. We used the narrow lines listed in Table 4 and the narrow component of the Hβ line which can be found in the spectra published by Boroson et al. (1985), de Robertis (1985) and de Waard (1986) (average luminosity $0.34\,10^{35}$ W). We compared the line ratios with the calculation of Stasińska (1984). A value for U of $5\,10^{-4}$ and $n_e = 5\,10^{-11}$ m^{-3} follows, with a typical scatter for individual line ratios of a factor 2 and 10 respectively. Additional uncertainty in the parameters arises due to the uncertainty in the chemical abundances and the precise shape of the ionising continuum. The above values are derived for a powerlaw with photon index 2.5. Normalising this spectrum to the UV flux of Fig. 2, we obtain $Q(H) = 4\,10^{55}$ photons/s. We obtain a typical radius of the narrow line region of $7\,10^{18}$ m, with an uncertainty of a factor 5.

If one assumes pressure equilibrium between the narrow line clouds (take a typical temperature of $2\,10^4$ K) and a hot confining medium, situated at a distance $r = 7\,10^{18}$ m from the central source and with a relative thickness Δ, it is possible to calculate the thermal bremsstrahlung X-ray flux from the confining medium, given its temperature. At maximum $\Delta = 1$ all observed low energy X-rays (Sect. 3) can be explained by a temperature of $5\,10^7$ K. At 10^8 K, only 20% can be explained by this mechanism. On the other hand, for lower temperatures Δ must be significantly smaller than 1 in order not to let exceed the predicted bremsstrahlung flux the observed X-ray flux.

2.4.3. Broad line region

The line fluxes of the broad lines are given in Table 4. We compare the observed line fluxes with the calculations of Kwan (1984). The ionisation parameter Γ is defined by

$$\Gamma = L_{\nu_L}/8\pi r^2 hcn \quad (8)$$

where n is the cloud density, r the distance to the central source, and L_{ν_L} the luminosity of the central source per frequency unit at the Lyman limit ν_L ($3.3\,10^{15}$ Hz). Kwan takes as the spectrum of the central source a powerlaw with energy index -0.5 below the Lyman limit, -2 from the Lyman limit to 100 eV and -0.5 above 100 eV. If we fit this spectral shape to the optical/UV Continuum of III Zw 2 at July 1977 (Fig. 2) we obtain a Lyman limit luminosity of $7\,10^{22}$ W Hz^{-1}. The observed hard X-ray flux of III Zw 2 however is a factor of 10 larger than predicted by this model.

The O I 1304/Ly α ratio is sensitive to variations in the product $n\Gamma$, and does not depend very much on other parameters. From the observed ratio and Fig. 5 of Kwan we deduce $n\Gamma = 1.2\,10^{14}$ m^{-3}. If we compare the observed hydrogen ratios (including Ly α, Hα, Hβ, Hγ and Pα) with Fig. 1 of Kwan, we find that his models 1, 2 and 5 disagree completely with the observed ratios, hence n must be typically larger than $2\,10^{15}$ m^{-3} and Γ larger than 0.03. On the other hand, the C IV/Ly α ratio suggests $\Gamma < 0.05$. As a typical value, we will adopt $\Gamma = 0.04$, corresponding to $n = 3\,10^{15}$ m^{-3}. From Eq. (8) we derive a distance of $1.1\,10^{16}$ m. Several uncertainties in the physical parameters of the Broad Line Region (BLR) clouds exist, however. First, the ionising continuum is variable. For III Zw 2, this can be a factor of 2. Furthermore, as we have stated already, the input spectrum of Kwan does not match the X-ray continuum. The broad lines are also variable. The lines for which we have at least 4 measurements at different epochs (Hβ, Ly α, C IV) show variability of the order of 20–30%. This may be smaller than the continuum variability due to the fact that the line intensities are averages over 2 years (the light-travel time through the region), while the variability time scale of the continuum is somewhat smaller (Sect. 2.2). There are also differences in the predicted line strengths as calculated by different authors. And finally, there may be different kinds of clouds emitting the broad lines (see e.g. Collin-Souffrin et al., 1986).

Krolik et al. (1981) have made calculations for the possibility that the broad line clouds are confined by a hot, low density medium. If we apply their calculations to III Zw 2, we find that the intercloud temperature is $1.0\,10^8$ K, if inverse Compton heating is the main heating mechanism of the intercloud medium. If other heating mechanisms are active, this temperature may rise to 10^9 K (in case those other mechanisms deliver ten times more energy than the inverse Compton process). Neglecting those other heating mechanisms, we find from the condition of pressure equilibrium an intercloud density n_{hot} of $6\,10^{11}$ m^{-3}.

We can calculate the thermal bremsstrahlung X-ray flux emitted by the intercloud medium: assuming that the intercloud medium fills a sphere with radius $1.1\,10^{16}$ m completely, we derive a total luminosity of $5\,10^{36}$ W. This luminosity is small compared to the observed X-ray flux from III Zw 2 (Sect. 3). In the energy range of 1–10 keV the hot intercloud medium contributes at most 10% to the total observed X-ray flux per keV. If extra heating occurs, however, the predicted intercloud flux is completely negligible; similarly, if the relative thickness of the broad line region is significantly smaller than 1, its X-ray flux is small. We conclude that the hot intercloud medium can be excluded as a source of hard or soft X-rays.

The optical depth for Compton scattering in the intercloud medium, defined by

$$\tau_{cs} = n_{hot}\sigma_T r \quad (9)$$

is 0.4 in the present case. As a result, rapid X-ray flux variations from the central source will be distributed partially over a typical timescale of 10 months, unless the relative thickness of the intercloud medium is smaller than one or extra heating occurs, in which case τ_{cs} is smaller. This seems to be the case, since the X-ray observations presented in Sect. 3 show a deep and fast eclipse at 2 keV, which yield an upper limit to τ_{cs} of about 0.10 ± 0.15.

Fabian et al. (1986) investigated an intercloud medium with a much lower temperature of 10^6 K due to an extra soft X-ray component of the central source. If we apply these calculations to III Zw 2, we find that the broad line region should have a thickness of at most 10^{13} m, otherwise the intercloud bremsstrahlungs flux is larger than the observed soft X-ray flux (Sect. 3). This thickness seems to be unrealistically low, hence we conclude that in the case of III Zw 2 such a low intercloud temperature is unlikely.

We next consider the kinematics of the broad line region clouds. In Fig. 3 we show the intensity profiles of 4 of the strongest

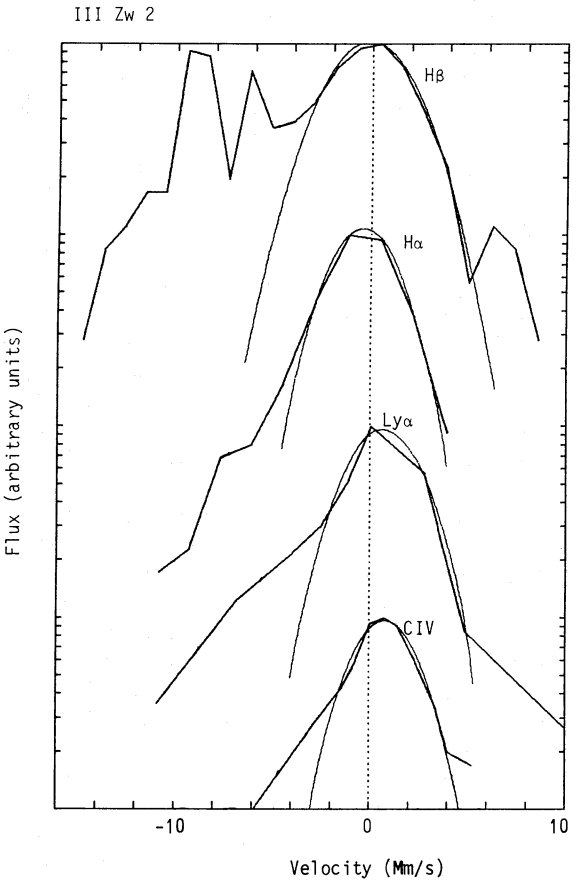

Fig. 3. Line profiles in III Zw 2. Thick curves: observed profiles; thin curves: model fits, to the central parts of the lines, as described in the text

lines. The data have been reduced to the rest-frame of III Zw 2. The Hα and Hβ profiles were taken from the tables of De Bruyn and Sargent (1978) while the Ly α and C IV 1549 line were taken from the figure in Chapman et al. (1985). For the Balmer lines we subtracted a linearly varying background, and for both UV lines we subtracted the average background (constant in W/Å) as given by Chapman et al.. We did not subtract the [O III] 4959 and 5007 lines, which are clearly visible and superimposed on Hβ. These lines are narrow, however, and do not disturb the central part of the Hβ line. From the work of de Robertis (1985) it follows that the relative contributions of Fe II lines to the red wing of Hβ become important (~20%) at a velocity of $-4000\,\mathrm{km\,s^{-1}}$; near the oxygen lines and in the extreme red wing its contribution is of the order of 50%. We also did not subtract these iron features. The zero point of the velocity scale is determined by the redshift of III Zw 2, obtained from the narrow lines (de Robertis, 1985).

It can be seen from Fig. 3 that the UV lines are blue-shifted with a mean velocity of $800\,\mathrm{km\,s^{-1}}$. This is consistent with the findings of Wilkes (1986) for a large sample of quasars, where the average blueshift was $600\,\mathrm{km\,s^{-1}}$.

The profile of Ly α is similar to the C IV profile. It has been argued (see, e.g., Carswell, 1985) that this can be explained by a model where most of the intensity of these lines arises in clouds which are not very optically thick. In that case the other lines like Hα, Hβ should be emitted by a different medium (Collin-Souffrin et al., 1986).

We made a first-order approximation to the kinematics of both types of clouds by using the following model. The clouds are in a thin spherical shell with a distance r to the central source and have a radial velocity v_r (either positive or negative). An opaque accretion disk with a radius r_d obscures the emission from clouds behind the disk. The clouds are assumed to emit isotropically. The resulting line profile is convolved with a Gaussian with a standard deviation σ. The resulting line shape depends upon 3 parameters: $\rho \equiv r_d/r$, v_r and σ. We fitted these parameters for the part of the line profiles with $|v| < 4000\,\mathrm{km\,s^{-1}}$ (the UV lines) respectively $|v| < 3000\,\mathrm{km\,s^{-1}}$ (the Balmer lines).

For the UV lines we obtain a typical value $\sigma = 1700$–$1900\,\mathrm{km\,s^{-1}}$, $v_r = 1400$–$1700\,\mathrm{km\,s^{-1}}$ (outflow) and $\rho = 0.99$–1.0. The Balmer lines show no blueshift, and they are fitted by a model with an inflow velocity of 1000–$1400\,\mathrm{km\,s^{-1}}$, velocity dispersion of 1700–$2200\,\mathrm{km\,s^{-1}}$ and ρ between 0.8 and 0.9. It follows that the Balmer line emitting clouds have a larger distance to the central source than the Ly α clouds.

From Fig. 3 we see that the model explains the central part of the lines reasonably. All lines however show a strong red wing which is not explained by the present model. For the Hβ line this wing is visible up to $15000\,\mathrm{km\,s^{-1}}$. The red wing in the Balmer line clouds may be explained by a small amount of clouds at smaller distances than most clouds, resulting in a complete occulation by the disk for clouds in the far blue wings of the lines. These extra clouds have larger infall velocities than the clouds which cause the central part of the Balmer lines.

It has been proposed (e.g., van Groningen, 1983) that a part of the broad lines in quasars may be due to emission from the accretion disk. If in the case of III Zw 2 a significant fraction of the line width is due to a rotating disk, velocities of $10^7\,\mathrm{m\,s^{-1}}$ at a distance of $10^{16}\,\mathrm{m}$ imply a central mass of at least 10^9 solar masses. The X-ray data which will be discussed in the next sections are inconsistent with such a large mass.

2.5. Previous X-ray observations

The X-ray radiation of III Zw 2 was detected by SAS 3 in 1977 (Schnopper et al., 1978) with a 2–10 keV luminosity of $1.4\,10^{38}\,\mathrm{W}$. It was observed in 1977–78 by HEAO 1 A-2 (Piccinotti et al., 1982), in 1979 by Ariel VI (Hall et al., 1981) and by Einstein in 1979–1980 (Petre et al., 1984).

The spectrum is fitted by a single powerlaw with a photon index of 1.3 ± 0.3 (SAS 3). The Ariel VI data (Hall et al., 1981) give a somewhat larger index of about 1.7, mainly because the neutral column density in this fit is rather large, $(9 \pm 6)\,10^{25}\,\mathrm{m^{-2}}$. The Einstein SSS data (Petre et al., 1984) yielded an upper limit to the column density of $7\,10^{25}\,\mathrm{m^{-2}}$ and an upper limit to the covering factor of the cool clouds of 68%. The photon index was 1.7 ± 0.4. Within the observational errors also a spectrum with only galactic absorption (column density $4\,10^{24}\,\mathrm{m^{-2}}$, Heiles, 1975) is possible. Such a fit has a spectral index of 1.3.

X-ray variability of III Zw 2 on the timescale of a year was reported first by Huchra et al. (1981). Later on, variability on a timescale of a day (doubling time 60000 s), was reported by Urry et al. (1986), based upon Einstein observations. These variations agree with the X-ray luminosity – time constant correlation as found by Barr and Mushotzky (1986). Recently, much faster variations have been reported from observations with EXOSAT. Kaastra and de Korte (1986) reported a fast absorption with a typical timescale of 5000 s, which will be discussed in detail in the next section, while Pounds (1986) reported a flare with a rise time of 1000–1500 s and a decay time of 3000–4000 s. The flare was twice as bright as the preflare continuum and was not visible at low energies (Exosat's LE detector). The flare softened during its evolution. The implications of these EXOSAT observations will be discussed in Sect. 4.

3. EXOSAT observations

3.1. Detection

III Zw 2 was observed by EXOSAT on December 18, 1983, from 12^h UT to 16^h30 UT. The instrument is described in detail by de Korte et al. (1981) and Turner et al. (1981); we used data from the Channel Multipler Array (CMA) of the low energy experiment (LE) and the argon counters of medium energy experiment (ME), which are sensitive in the energy ranges 0.05–2 and 1.5–35 keV, respectively.

The LE has a spatial resolution of 18′ but provides no spectral information. Spectral information can be obtained only by using filters in combination with the CMA. The 400 nm Lexan filter was used before 15^h UT and the 300 nm Lexan filter afterwards. Besides III Zw 2 the B9 V star 34 Pisces was also detected by the LE. This 5.5 magnitude star has a strong UV flux and the mean (background subtracted) count rate obtained with the 400 nm and 300 nm filter of 0.020 ± 0.002 and 0.121 ± 0.006 cts/s, respectively, is typical for stellar UV contamination in the LE. The flux as determined by the ME experiment is not sensitive to UV contamination. Furthermore, although 34 Psc is a double system, the separation between the B9 star and its faint red companion ($10^{14}\,\mathrm{m}$) is so large that accretion driven X-ray emission can be excluded. We conclude that 34 Pisces is not expected to disturb the ME spectrum of III Zw 2.

The ME consists of 2 similar halves, of which one half monitored III Zw 2 and the other half a neighbouring region without known X-ray sources. The contribution of the background X-ray

radiation and of the particle induced background was subtracted from the spectrum by using observations of sky regions without X-ray sources during the slew towards and away from III Zw 2; slow and weak (<0.5%) variations in the particle background during the observation of III Zw 2 could be traced using the offset ME half, and the source count rates were corrected for these variations.

3.2. *X-ray time profile*

The resulting light curve for III Zw 2 is shown in Figs. 4 and 5. The ME count rate decreases until 14^h30 and rises afterwards. The corresponding variability range of about 30% is significant at the 0.1% confidence level. This confidence was calculated from an F-test on the hypothesis that both the linear and quadratic term in a parabolic fit to the count rates as a function of time are zero. Such a parabolic fit appears to be sufficient to describe the present data; the residuals have a χ^2 of 11.5 for 13 degrees of freedom.

The LE light curve (which was also corrected for weak background variations) is different and appears to be uncorrelated with the ME light curve. However, variability in the LE on a timescale of an hour cannot be excluded at the 2.5% and 5% confidence level for the 400 nm and 300 nm filter, respectively. The mean count rates in both filters are 0.008 ± 0.002 and 0.015 ± 0.003 cts/s, respectively.

We investigated which part of the ME spectrum contributed most significantly to the total variability. It is evident from Fig. 5 that the variability originates at energies below 3 keV and above 4 keV. In both energy ranges the variability pattern of Fig. 5 is followed, with different amplitudes however. Between 3 and 4 keV the spectrum is constant. Alternatively, we plot in Fig. 6 the ratio of the spectrum during minimum to the spectrum during maximum; both time intervals are defined in the next section. This figure also shows that the effective "transmission" at 1.5 keV is nearly zero, near 3 keV the spectrum is constant and at higher energies there is also a significant intensity drop.

We checked whether instrumental effects might be responsible for the observed variations. Experience with observations of other sources with the ME shows that the data above 1.5 keV which were used here are reliable. Furthermore, the typical time profile below 2 keV was not a special feature of one of the energy channels in one of the counters of the ME, but all relevant data channels showed the same tendency. Finally, the variations in the particle background counting rate which were removed from our data were uncorrelated with the final lightcurve, which confirms that the measured time variability cannot be due to background variations.

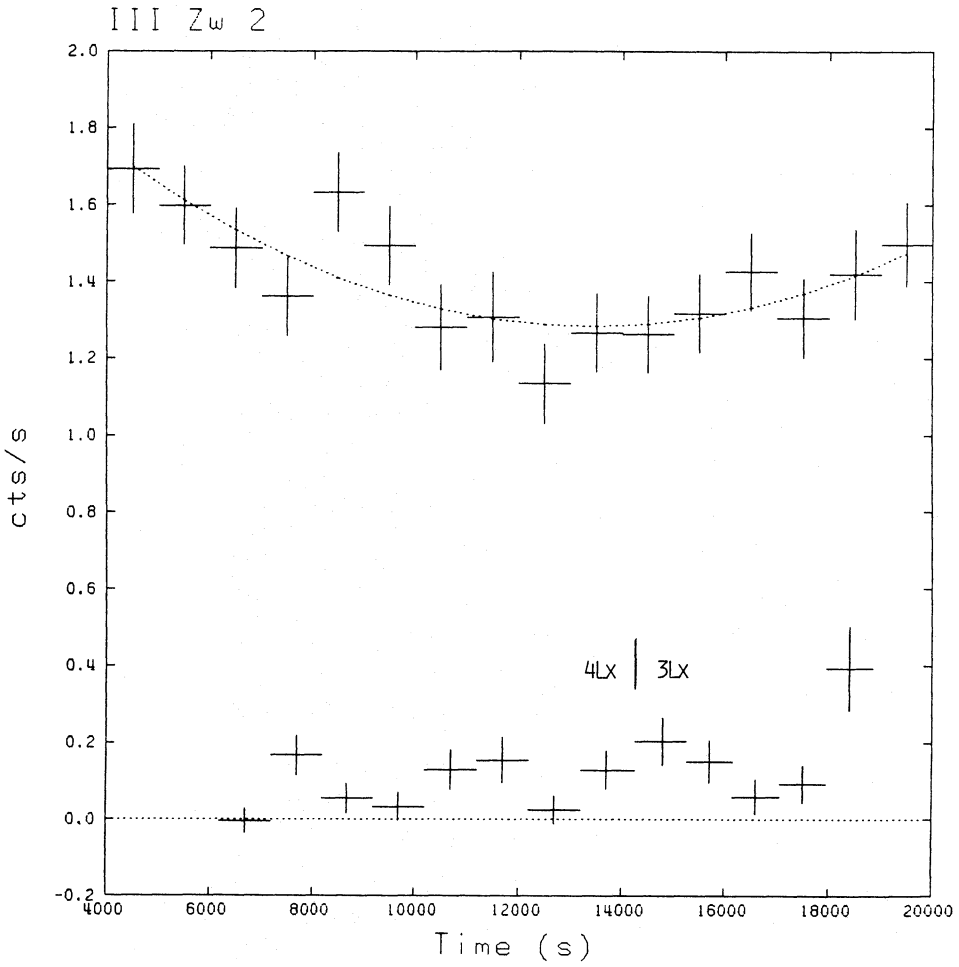

Fig. 4. 1.5–10 keV time profile of III Zw 2 with the ME experiment (upper curve) and LE experiment (lower curve multiplied by a factor of 10). Note the filter change in the LE at 14000 s. The upper dotted line is the best fitting parabola to the ME data

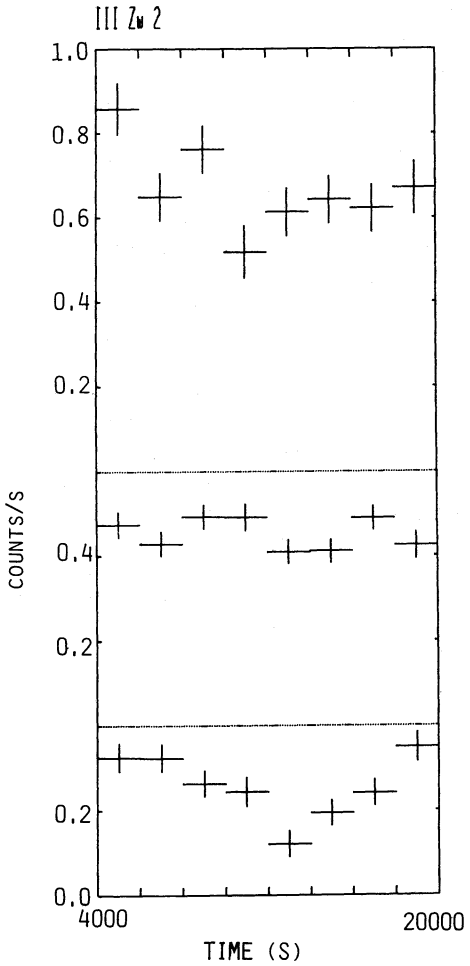

Fig. 5. Time profile of III Zw 2 with the ME experiment in different energy bands. Lower panel: 1.3–2.5 keV; Middle panel: 2.5–4.1 keV; Upper panel: 4.1–9.7 keV

3.3. Spectral fitting

The spectrum of III Zw 2 was determined in the energy range 1.6 to 9.7 keV. The ME spectra at the beginning and end of the observation showed no significant differences. Therefore we averaged the first 3000 s and the last 2000 s of the observation, and took this as representing the "maximum" spectrum. This maximum spectrum (Fig. 7) could be fitted by a power law with photon index 1.35 ± 0.15, intrinsic (i.e. redshift corrected) 2–10 keV luminosity of $(6.6 \pm 0.3)\,10^{37}$ W and a standard neutral hydrogen column density corresponding to extinction by our own galaxy of $4\,10^{24}\,\mathrm{m}^{-2}$ (Heiles, 1975), with a 1σ upper limit of $6\,10^{25}\,\mathrm{m}^{-2}$. Errors indicate 1σ limits. The fit is quite satisfactory ($\chi^2_{22} = 20.1$). The absorption cross section was taken from Morrison and McCammon (1983). The power law index agrees with the earlier measurements by SAS-3 (Schnopper et al., 1978) and also with the Ariel VI (Hall et al., 1981) and Einstein (Petre et al., 1981) data, taking into account the larger value of n_H (close to our upper limit) which was used in those papers.

We turn to the "minimum" spectrum (Figs. 8 and 9). We selected a time interval of 5000 s centered around 14^h30, corresponding to the ME datapoints 7–11 in Fig. 4. The spectrum was fitted (Fig. 8) by a powerlaw with photon index $1.85\,(-0.2, +0.75)$, 2–10 keV luminosity of $6.3\,(-0.1, +1.4)\,10^{37}$ W and an extra, cosmologically redshifted internal column density of $1.8\,(-0.7, +2.7)\,10^{26}\,\mathrm{m}^{-2}$ above the galactic (unredshifted) column density of $0.04\,10^{26}\,\mathrm{m}^{-2}$. The goodness-of-fit is $\chi^2_{22} = 33.5$. The listed errors on the strongly correlated photon index and internal column density are combined 1σ limits. The photon index is larger than the photon index of the maximum spectrum at the 2% confidence level (see Fig. 10).

Alternatively, the minimum spectrum was fitted by a powerlaw with absorption by our galaxy as before and extra absorption by a hot and dense partially unionized cloud (Fig. 9). This model is discussed later on (Sect. 4.2). The best fit is obtained for a powerlaw with the same photon index as during maximum (1.35 ± 0.15) but a smaller intrinsic 2–10 keV luminosity of $(5.1 \pm 0.3)\,10^{37}$ W. The goodness-of-fit is slightly better than for the cool absorber: $\chi^2_{22} = 33.0$. The hot absorber has a column density of $(8 \pm 3)\,10^{27}\,\mathrm{m}^{-2}$ and an inflow velocity of $(0.5 \pm 0.1)c$. Both models are discussed in detail in Sect. 4.2.

The effective energy band for the LE flux is 0.5–1.0 keV if the spectrum is fitted by the ME maximum spectrum. The LE count rate is consistent with this best fit maximum spectrum, if no internal absorption occurs. In case of a cool absorber, the contribution of the "minimum" powerlaw component to the LE count rate is negligible compared to the observed count rate. Contrary, in the hot absorber case, we expect the LE count rate of the powerlaw component during minimum to be about 70% of the count rate during maximum. This is consistent with the present data.

4. Interpretation of the X-ray data

4.1. Variability and spectrum

The main results of the present observations to be explained are:

1. The fast variability time scale.
2. The strong intensity reduction below 2.5 keV
3. The intensity reduction above 4 keV.
4. The different time dependence in the LE energy band.

We interpret the present variability by a model in which an absorbing object passes the central X-ray source and intercepts a part of the X-ray flux for a while, cf. our spectral fits in Sect. 3.3. We will discuss the absorber and the absorbing mechanism in more detail later on (Sect. 4.2); for this moment we only need to know the absorber radius R_a and its transverse velocity v_t.

At low energies the effective transmission of the radiation during minimum is nearly zero (Fig. 6). This indicates that the absorber is larger than or at best as large as the X-ray source, otherwise the eclipse would have been less pronounced at these low energies. On the other hand, we do not expect the X-ray source to be much smaller than the absorber, for in that case the transmission is expected to drop very fast during the first part of the eclipse, and to be rather constant during the rest of the eclipse duration. Our more gradual time profile better agrees with an X-ray size which is of the same order of magnitude as the absorber size. Furthermore, the total duration of the depression in flux (about 10000 s) can be used to derive the radius R_a of the absorber using its transverse velocity v_t.

It then follows for the X-ray source radius R_X:

$$R_X \lesssim R_a \simeq (v_t/c)\,1.5\,10^{12}\,\mathrm{m}\,. \qquad (10)$$

Accretion onto compact active galactic nuclei can occur in several forms. Blandford (1985) has given a review on this subject. The

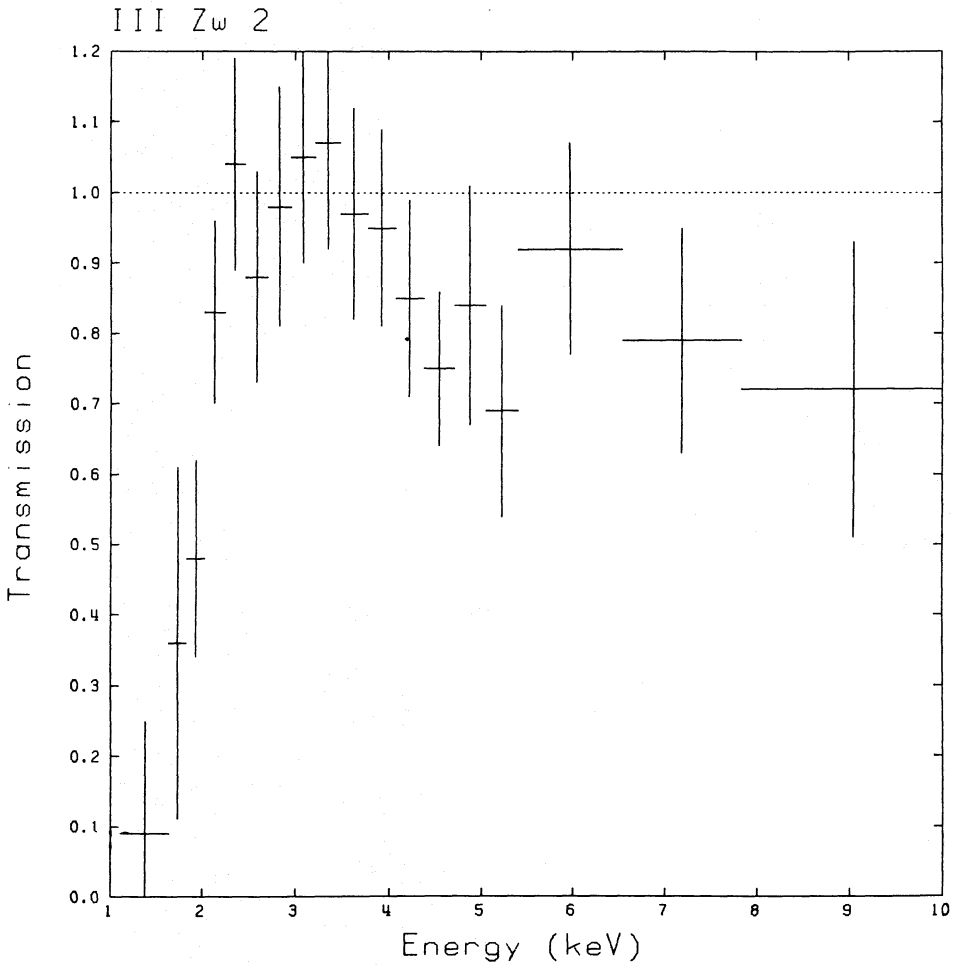

Fig. 6. Effective transmission in III Zw 2 during minimum. The ratio of the "minimum" spectrum (Figs. 8 and 9) to the "maximum" spectrum (Fig. 7) is plotted. Note the strong reduction below ~2 keV and the reduction above 4 keV.

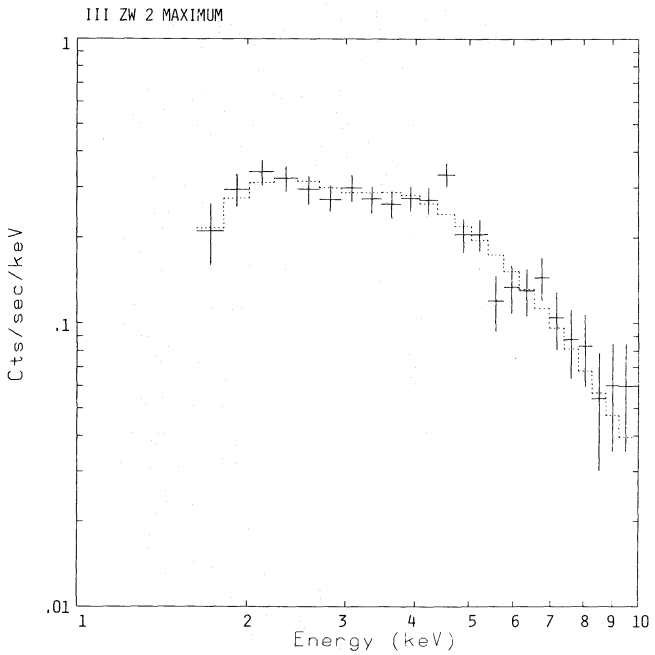

Fig. 7. Maximum spectrum of III Zw 2. The spectrum of the first 3000 and last 2000 s was fitted by a powerlaw (dashed line) with parameters given in the text.

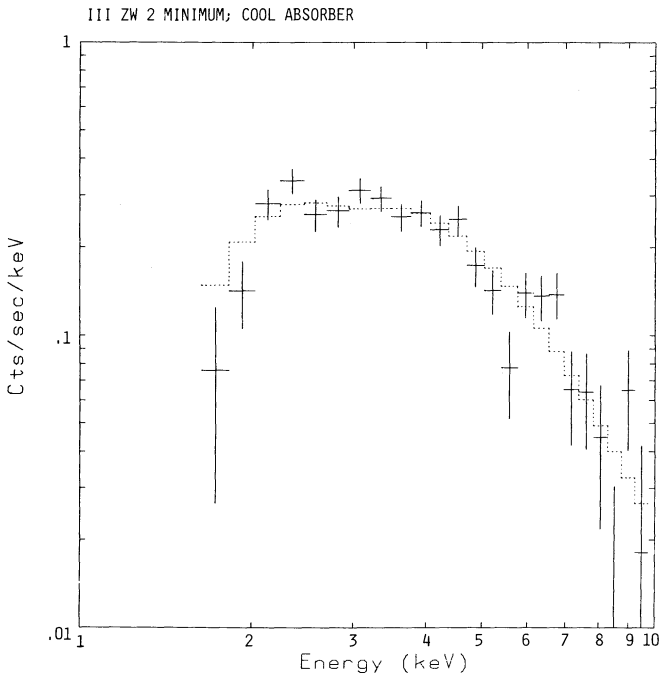

Fig. 8. Minimum spectrum of III Zw 2. The spectrum between 6000 and 11000 s after the start of the observation was fitted by a powerlaw plus extra absorption by a cool absorber (dashed line) as described in the text

critical parameter is the dimensionless accretion ratio $\dot{m} = \dot{M}c^2/L_{\rm Edd}$. If this parameter is smaller than 0.1, the accretion occurs in the form of an ion torus; for $0.1 \lesssim \dot{m} \lesssim 10$ an accretion disk can be maintained; at a ratio of 10 this disk will thicken because of radiation pressure and a radiation-torus develops; finally for $\dot{m} \gtrsim 100$ the accretion is super-critical and strong outflows may result. We restrict our present discussion to the case of an accretion disk, either thin or thick, corresponding to $0.1 \lesssim \dot{m} \lesssim 100$.

In the case of a thin disk, the accretion disk may extend down to the last stable circular orbit around the central black hole, and we expect the X-ray source to have at least that radius; contrary, for a thick disk, the X-ray radiation can be expected to fill a large fraction of the funnel of the torus, which could have an opening diameter of typical 100 Schwarzschild radii if e.g. the model of Sikora (1981) is used. In the case of a thick disk due to the presence of a funnel the outcoming X-ray radiation may also show a considerable degree of beaming. For both the thick and the thin disk case we will adopt a lower limit to the X-ray radius of 3 Schwarzschild radii, i.e.

$$R_{\rm X}/R_{\rm S} \gtrsim 3\,. \tag{11}$$

The observed 2–10 keV luminosity is related to the total luminosity L by the bolometric correction b:

$$b \equiv L/L_{2-10}\,, \tag{12}$$

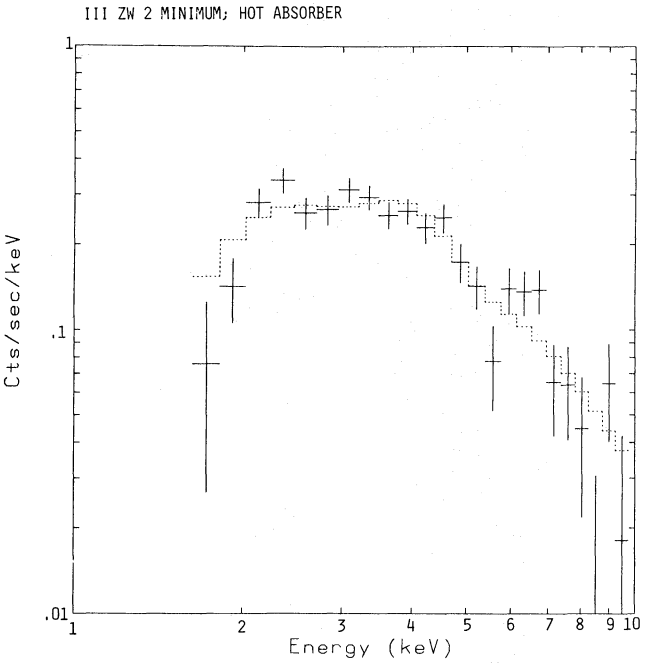

Fig. 9. Minimum spectrum (as in Fig. 8) but fitted by a redshifted hot absorber

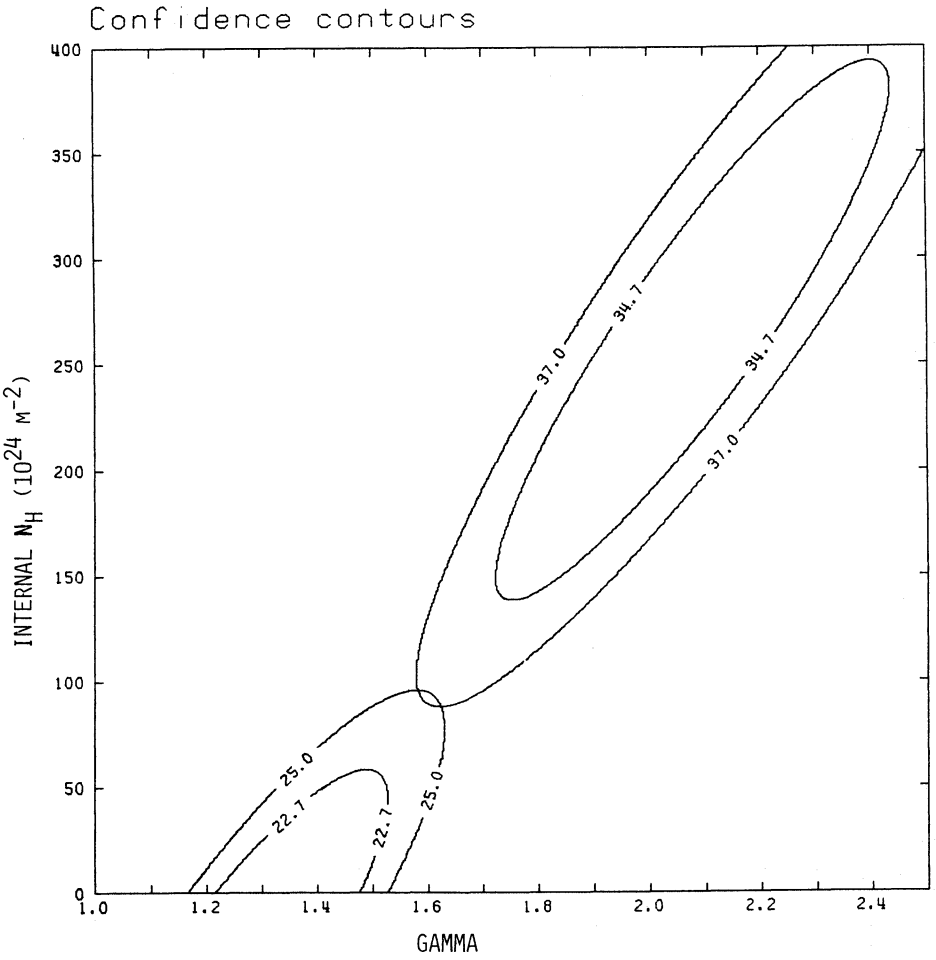

Fig. 10. 1σ and 90% confidence contours for the internal column density and the photon index, in case of a cool absorber. Lower left: maximum spectrum (Fig. 7); upper right: minimum spectrum (Fig. 8)

while L itself may be expressed in units of the Eddington luminosity by defining

$$f \equiv L/L_{\rm Edd}\,. \tag{13}$$

Inserting the observed 2–10 keV luminosity during maximum into the above expressions yields the mass of the central object:

$$M = 5\,10^6\, b/f M_\odot\,. \tag{14}$$

The observed X-ray spectrum may be represented by a powerlaw and we will assume here that it is caused by inverse Compton scattering from soft photons off a thermal distribution of electrons. We need to specify the source of soft photons. In principle, the bremsstrahlung photons produced by the thermal electrons could be used as the soft photons. Apart from a possible Wien peak the resulting X-ray spectrum is very hard, however, with an energy index equal to 0 up to the Wien peak (Felten and Rees, 1972). Therefore we consider another source of soft photons, namely the blackbody emission from the accretion disk. A disk with a temperature T produces a hard X-ray spectrum per unit area of (energy/area/time/energy):

$$\frac{15\alpha\Gamma(\alpha+4)\zeta(\alpha+3)}{2\pi^4(2\alpha+3)}\,\frac{\sigma T^4}{kT}\left(\frac{kT}{E}\right)^{\alpha}, \tag{15}$$

which follows from the expressions given by Sunyaev and Titarchuk (1980). Here E is the photon energy, σ is the constant of Stefan-Boltzmann, Γ is the gamma-function and ζ is Riemann's ζ-function. The energy index α is given by

$$\alpha = \left\{\frac{9}{4} + \pi^2\left[3\theta\left(\tau_{\rm p} + \frac{2}{3}\right)^2\right]^{-1}\right\}^{1/2} - \frac{3}{2}, \tag{16}$$

where $\tau_{\rm p}$ is the optical depth due to Compton scattering and θ the dimensionless electron temperature, defined by

$$\theta \equiv kT_{\rm e}/m_{\rm e}c^2\,. \tag{17}$$

For α we substitute the value during maximum, 0.35 ± 0.15, which is also the value during minimum in the hot absorber case. In case of a thick disk, the total emitting area of the soft photon source is given by the area of the funnel; in case of a thin disk it is $2\pi R_{\rm X}^2$, where the factor two arises from emission from both sides of the disk. We generalise these results by taking the effective area A as follows:

$$A = 2\pi R_{\rm X}^2/\sin\phi\,, \tag{18}$$

where ϕ is half the opening angle of the funnel.

In case of a thick disk funnel, not all the X-rays can escape; a part is re-absorbed by the funnel walls. We estimate the escaping fraction by $1 - \cos\phi$, which is just the solid angle sustended by the two funnels, divided by 4π. The total luminosity escaping from the source is also a fraction $1 - \cos\phi$ of the inferred 2–10 X-ray luminosity deduced from the flux at earth assuming isotropic emission (we look into the beam). Finally, by comparing the inferred 2–10 keV luminosity of $6.6\,10^{37}$ W with the predicted X-ray flux we obtain the following relation:

$$L_{2-10} = \frac{15\alpha\zeta(\alpha+3)\Gamma(\alpha+4)\sigma T^4 R_{\rm X}^2}{\pi^3(2\alpha+3)(1-\alpha)\sin\phi}\left[\left(\frac{10\,\text{keV}}{kT}\right)^{1-\alpha} - \left(\frac{2\,\text{keV}}{kT}\right)^{1-\alpha}\right]. \tag{19}$$

Another condition on the X-ray source can be obtained from the flare properties of III Zw 2. Under the same conditions where (16) holds, i.e. $\theta \ll 1$, $\tau_{\rm p}^2 \gg 1$, the diffusion of photons was modelled by Sunyaev and Titarchuk (1980). If at the centre of the X-ray source due to some process extra hard X-ray photons are produced, these photons will be scattered in the optical thick central source before escaping. The distribution of arrival times of the photons is characterised by a steep, non-exponential increase until the maximum is reached, followed by a more gradual exponential decay. The decay time as given by Sunyaev and Titarchuk (1980) is:

$$t_{\rm d} = 3(\tau_{\rm p} + 2/3)^2 R_{\rm X}/\pi^2\tau_{\rm p}c\,. \tag{20}$$

The X-ray flare observed by Pounds (1986) is now interpreted in terms of such a diffusion model. In the model of Sunyaev and Titarchuk, the ratio of the $1/e$ risetime to $1/e$ decay time is 0.4. This ratio agrees with the ranges for the rise and decay times as given by Pounds (1986). It is also clear that the flare must soften during its decay, as the observations show, for photons which arrive later have been scattered more often and hence have lost more energy. Now by comparing the observed exponential flare decay time of 2900 ± 400 s (Pounds, 1986) with (23) we obtain a relation between $R_{\rm X}$ and $\tau_{\rm p}$. We demand further that the accretion disk extends to the last stable circular orbit around the black hole, with the mentioned distance of 3 Schwarzschild radii. This corresponds to an accretion efficiency of 5.7%. The efficiency is defined by:

$$\varepsilon \equiv L/\dot{M}c^2\,. \tag{21}$$

Finally, we may derive the bolometric correction b from the exact expression of the X-ray spectrum at energies comparable to the temperature of the electrons, as given by Sunyaev and Titarchuk (1980). The bolometric correction is given by

$$b = \frac{\Gamma(1-\alpha)\Gamma(4+\alpha)\Gamma(\alpha)(1-\alpha)\theta^{1-\alpha}}{\Gamma(2\alpha+3)\left[Y_{10}^{1-\alpha} - Y_2^{1-\alpha}\right]}. \tag{22}$$

where $y_{\rm E} = E/511\,\text{keV}$.

The last condition is obtained from the optical properties of the accretion disk, which yielded (Sect. 2.2):

$$M\dot{M} = (1.1 \pm 0.4)\,10^8\, M_\odot^2\,\text{yr}^{-1}\,. \tag{23}$$

We note that the uncertainty in this parameter is mainly due to the variability of III Zw 2.

The parameters of III Zw 2 are derived using Eqs. (13)–(14) and (16)–(23). We may first put a few constraints on the parameters. First, the observed hard X-ray spectrum extends to at least 10 keV. The calculated spectrum (Sunyaev and Titarchuk, 1980) starts deviating significantly from a powerlaw at 10 keV for temperatures below 5 keV. Therefore the first constraint is

$$\theta \gtrsim 0.01\,. \tag{24}$$

Furthermore, we expect the transverse cloud velocity not to be much larger than $0.5\,c$. This limits the X-ray radius to

$$R_{\rm X} \lesssim 7.5\,10^{11}\,\text{m} \tag{25}$$

The accretion disk temperature at the X-ray source is not expected to be lower than the maximum temperature of the disk derived from the optical UV data, resulting in:

$$T_{\rm d} \gtrsim 35000\,\text{K}\,. \tag{26}$$

The spectral index is given by (16), which is valid for

$$\tau_{\rm p}^2 \gg 1\,. \tag{27}$$

Table 5. Typical parameters for the X-ray source of III Zw 2

Parameter	Value
Total luminosity	$8\,10^{38}$ W
Optical depth	8
Radius	$3\,10^{11}$ m
Gas density	$4\,10^{17}\,m^{-3}$
Temperature	$2\,10^{8}$ K
Central mass	$5\,10^{7}\,M_{\odot}$
Accretion rate	$2\,M_{\odot}\,yr^{-1}$
Maximum relative thickness disk	0.8
Effective X-ray beaming	50°

Finally, we do not expect the luminosity to be much larger than the Eddington luminosity, otherwise the accretion process will stop. This condition may be written as

$$f \lesssim 1 . \qquad (28)$$

The set of limiting equations for III Zw 2 consists of (11) and (24)–(28).

It appears that (11) and (28) are the most restrictive conditions. Only a rather narrow parameter range is allowed. Its precise range depends upon the observational errors on the several observable variables and even the adopted value of Hubble's constant is important. The deviations are not much larger than at most a factor of 2, however. In Table 5 we list a typical set of parameters. The conclusions of our paper are essentially unaffected by shuffling a little with these error bounds.

The electron temperature derived is $2\,10^{8}$ K. This temperature implies a cut-off in the hard X-ray spectrum at about 100 keV. Future X-ray missions should be able to observe that cut-off. The radius of the X-ray source is about 3 times the Schwarzschild radius. The absolute value of the radius is $3\,10^{11}$ m. If we combine this radius with the optical depth in the X-ray source, we obtain a density of $4\,10^{17}\,m^{-3}$. The central mass of III Zw 2 is $5\,10^{7}\,M_{\odot}$, while the accretion rate is $2\,M_{\odot}\,yr^{-1}$. If we combine both numbers, we find that the lifetime of the central black hole in III Zw 2 is rather small, some 20 million years. This implies that the activity has started only recently; the time scale is compatible with the typical crossing time of a companion galaxy with a velocity of $1000\,km\,s^{-1}$ over a distance of 20 kpc, the typical size of the parent galaxy. The maximum relative thickness of the disk is given by Shakura and Sunyaev (1973): $(h/r)_{max} = 0.037\,m$ which in our case equals 0.8. This corresponds to an opening angle of 50° for the "funnel". We see that the assumption of a thin accretion disk is hardly tenable in III Zw 2 and certainly deviations from the ideal Shakura-Sunyaev disks will be present in the central parts of the accretion disk. Because the maximum relative thickness of the disk is reached at a distance of 6.75 Schwarzschild radii and the X-ray source is smaller, the X-ray radiation will show some degree of beaming. For the present opening angle of 50° this implies that the fraction of space where the X-rays can be observed is $1 - \cos\phi \simeq 0.35$. The total X-ray luminosity is $8\,10^{38}$ W, where we used the bolometric correction $b = 12$. This luminosity is radiated at a rate close to the Eddington limit ($f = 1$).

It is possible to derive more information on the accretion disk using the model of Shakura and Sunyaev (1973). Firstly, from the observations of the broad line profiles we deduced that the accretion disk had a radius of typically 80–100% of the broad line region radius. For the disk radius we may take 10^{16} m therefore.

Collin-Souffrin (1987) has made calculations for the outermost and optical thin part of the accretion disk. If we extrapolate his calculations for $\alpha = 1$ and 10 to III Zw 2, we find that our observed disk radius equals the radius at which the disk becomes optically thin for a value of the disk parameter α typically of the order of 0.1.

Using that value, we find that in the interior of the disk radiation pressure dominates for radii below $4\,10^{14}$ m while gas pressure dominates outside; further, free-free opacity dominates the total opacity outside a radius of $8\,10^{15}$ m, which is beyond the observed disk radius. In the outer regions, however, self-gravitation of the disk becomes an important effect in the pressure balance of the disk. The gravitational acceleration due to the central black hole $g_z = GMz/r^3$ equals the acceleration due to self-gravity $g_s = 4\pi G\rho z$ (cf. Paczyński, 1978) at a distance in the order of $2\,10^{14}$ m for the value of α adopted presently. At this radius, instabilities are expected to occur; the typical timescale will be the dynamical timescale of the disk which is of the order of a year (the sound crossing time through the disk in the z-direction). This is equal to the observed optical flare decay time (Sect. 2). We note that the maximum emissivity per annulus in the B band occurs at radii smaller than the radius where self gravity becomes important, using the surface temperature distribution law (1). Because the dynamical timescale scales with $r^{3/2}$, any disturbances generated at that last radius with a characteristic timescale t_{dyn} will show up with the same time constant at smaller radii. It seems therefore natural to explain the optical B band variations by instabilities generated in the disk at the radius where self gravity becomes important. The total disk mass is of the same order of magnitude as the central black hole mass, which is another argument that the activity in III Zw 2 cannot have lasted longer than $2\,10^{7}$ years.

We note further that the observed optical/UV continuum showed a maximum temperature of 35000 K (Sect. 2.2), which corresponds to a radius of 10^{13} m. Apparently, we do not observe directly the thermal emission from the inner part of the accretion disk. A possible explanation can be found in magnetic effects. The infrared synchrotron source has also a size of the order of 10^{13} m (Sect. 2.3), while its luminosity is at least a few times larger than the observed disk component (in June 1978, during a flare, its luminosity was of the order of $1.5\,10^{39}$ W, if a low frequency cut-off at $10^{12.5}$ Hz is assumed, cf. Sect. 2.3). We suggest that the direct disk emission of the inner part of the disk is not emitted directly but reprocessed in the strong synchrotron source region. The magnetic pressure in the synchrotron source is about 1 Pa, but it may be two orders of magnitude larger if we take a cut-off frequency of 10^{13} Hz instead of $10^{12.5}$ Hz, resulting in only a twice as low synchrotron luminosity at the date considered. In that case, the magnetic pressure is of the same order of magnitude as the gas pressure in the disk at a radius of 10^{13} m. But if dynamo effects are active in the disk, the disk magnetic pressure may become even larger than in the synchrotron source and may compete with the disk radiation pressure of 10^{5} Pa at 10^{13} m. It is clear that magnetic effects play an important, if not dominating role in the disk dynamics.

4.2. The absorber

In Sect. 3.3 we fitted the minimum spectrum by two different models representing extreme cases for the temperature: one with a cool (10^4 K) absorber, the other with the hottest possible absorber of $\sim 9\,10^5$ K.

In the case of a *cool absorber* one might think of a broad line region cloud. Broad line region clouds have often been invoked as the absorbers which cause the long timescale variations in low luminosity Seyferts. Our fit to the minimum spectrum, as compared to the maximum spectrum, showed a similar or even higher 2–10 keV luminosity, but a much steeper power law index than during maximum. The number of ionising (XUV) photons during minimum is therefore much larger than during maximum. This will result in a temperature increase and a corresponding opacity decrease in the cloud. If the cloud remains in the line of sight, we then expect a decrease in column density contrary to observation, which shows a marked column density increase during minimum. On the other hand, it is very unlikely that at the same time that the source changes its spectrum, a distant cloud passes; and by the time the source is back in its former state, the absorber has disappeared. Finally, we note that during minimum the column density is that high that no flux is transmitted in the LE energy band. Any flux observed in the LE during minimum must originate in a separate spectral component. We may conclude therefore that a cool absorber yields no satisfactory explanation to the present data.

We next consider the *hot absorber* case. The absorbing object which causes the continuum reduction in III Zw 2 will be strongly influenced by the ionising continuum of the central source. The cloud can persist only if the ionisation heating is balanced by cooling processes, like radiative line cooling etc. (Krolik et al., 1981). Given the spectrum of the central source, only one or a few stable cloud temperature values exist. Assuming an input spectrum between 1 eV and 400 keV with energy index -1, Krolik and Kallman (1984) have calculated the equilibrium temperature and the corresponding opacity curve as a function of the ionisation parameter, defined by

$$\Xi = L/4\pi D^2 cnkT\,. \tag{29}$$

The stable low temperature branch exists for values of Ξ from 0 to about 33, corresponding to temperatures from 10^4 K to $9.16\,10^5$ K. At low temperatures, the opacity curve is similar to the one by Morrison and McCammon (1983); with increasing temperature, the opacity decreases rapidly, most significantly at low energies. At high temperatures also the ionisation edges due to several elements become pronounced: at about 0.9 keV the O-edge, between 1 and 2 keV the edges due to Mg, Si and S and at 8 keV the Fe-edge. The precise location of these edges depends upon the temperature; in general the edge energy increases with increasing temperature. At low temperatures, the resulting transmission increases smoothly with increasing energy, apart from a few weak edges. At a temperature of $9.16\,10^5$ K however, the transmission below the O-edge at 0.9 keV is 1; it becomes lower at higher energies, and reaches a minimum near the edges of Mg, Si and S; finally the Fe-edge causes a new strong transmission drop near 8 keV. The hot absorber model which we fitted to the minimum spectrum of III Zw 2 was the model with a temperature of $9.16\,10^5$ K. Models with a lower temperature did not result in an acceptable fit. As our fit in Sect. 3.3 showed, the slope of the power law component did not vary between the maximum and minimum spectrum. During minimum in addition to the absorption effect, the source intensity has dropped by $81 \pm 5\%$ while a cloud of column density $(8 \pm 3)\,10^{27}\,\mathrm{m}^{-2}$ passed between us and the central source.

The column density which we derived is very large and because the plasma in the cloud is almost completely ionised (apart from a few heavy elements) Thomson scattering of the X-rays on free electrons will be important. The Thomson optical depth from the centre of the cloud to its boundary derived from the total neutral column density is 0.45 ± 0.15. In that case, some 55% of the incoming radiation is not scattered. Some 40% is scattered once and 5% two or more times. If the incoming radiation is strongly beamed, we expect a continuum reduction of about 55% of the original level due to losses in the original direction caused by scattered photons. If, however, the incoming radiation has an extended angular distribution, like for example a semi-sphere, the radiation towards the observer does not only consist of directly transmitted, unscattered radiation but also of scattered radiation from other directions. In case of a semi-sphere the effective scattering-transmission then amounts to $\sim 80\%$, close to the observed value.

In the present analysis, we have assumed that the absorber has solar abundances. If, however, the abundance of the heavy elements like O, Mg, Si, S and Fe is larger by a factor of two, our estimate of the equivalent hydrogen column density of $8\,10^{27}\,\mathrm{m}^{-2}$ becomes smaller by a factor of two. This is because the absorption characteristics of an absorber with the temperature presently adopted are solely determined by the heavy elements, while the role of hydrogen and helium, which produce most of the free electrons can be neglected (Krolik and Kallman, 1984). Therefore, in the case of a twice as large heavy element abundance the Thomson optical depth of the cloud reduces to ~ 0.23 and then the observed continuum reduction of 80% can be explained by strongly beamed radiation into the direction of the observer, without invoking a continuous angle-distribution. We conclude that the observed continuum reduction of 80% can be explained by either Thomson scattering of strongly beamed radiation in a cloud with twice the solar abundance or scattering from a radiating semi-sphere in a cloud with solar abundances, or a combination of both models.

The column density of the absorber results in a gas density for the cloud of $4\,10^{15} c/v_t$, where v_t is the transverse cloud velocity (cf. Sect. 4.1). Now by substituting the density derived above, the temperature of $9.16\,10^5$ K, the ionisation parameter (33.2) and the luminosity ($8\,10^{38}$ W) and value for v_t/c (0.20) which follows from the X-ray radius obtained in Sect. 4.1, the distance to the central source can be derived from (29), resulting in

$$D = 1.6\,10^{14}\,\mathrm{m}\,. \tag{30}$$

This distance is much smaller than the distance of $1.1\,10^{16}$ m of the BLR clouds to the central source (Sect. 2.4). It is known however, that broader lines with higher ionisation degree are closer to the central object than cooler lines. Recently, a new, hotter ($\sim 10^5$ K) cloud component at one third of the BLR clouds distance was discovered in NGC 5548 (Peterson and Ferland, 1986). This component showed a velocity dispersion which was 75% larger than the line width of the other broad lines. The full width at zero maximum (FWZM) for the hot He II 4686 line was about 18000 km s^{-1} for NGC 5548. In the case of III Zw 2 the Hα line has already an FWZM of 17400 km s^{-1} (Osterbrock, 1977), so

if a similar hotter cloud region exists in III Zw 2, these clouds are expected to have a FWZM of about 30000 km s^{-1}. The hot cloud which we discuss in this paper is closer to the central source however than the clouds discussed by Peterson and Ferland and its temperature is also a factor of 10 higher.

Is it still possible that the present absorber is a cloud of the same population as the broad line region clouds? We need to know the maximum velocities the broad line region clouds may reach. The red wing of the UV and Balmer lines (Fig. 3) have an exponential behaviour $I \sim \exp(-v/v_w)$ up to at least 15000 km s^{-1} where the intensity becomes too low to be resolved. The velocity scale v_w is of the order of 3000 km s^{-1}. From the total number of clouds derived in Sect. 2.4 we expect clouds with velocities of the order of 70000 km s^{-1} to occur. This velocity is very large and approaches the present hot cloud radial infall velocity of $(0.5 \pm 0.1)\,c$. The transverse cloud velocity as derived from the X-ray data in Sect. 4.2 is a factor of two smaller than this radial velocity. This indicates that the cloud has a more or less radial orbit and that probably is the only reason that it could come that close to the central source. The cloud can only reach such a short distance to the X-ray source if braking by radiation pressure is unimportant. We consider braking by radiation pressure is unimportant. We consider braking due to Compton scattering and braking due to absorption of X-ray photons. The deceleration of the cloud due to Compton scattering and gravitation is given by

$$dv/dt = (1 - L/L_{\mathrm{Edd}})\,GM/D^2\,. \tag{31}$$

Taking L of order L_{Edd} and substituting for $M\,5\,10^7\,M_\odot$ as the X-ray data showed the acceleration at 10^{14} m is of the order of 0.1 m s^{-2}.

The time needed for the cloud to travel a distance of the size of the broad line region ($1.1\,10^{16}$ m) with a velocity of $0.5\,c$ is $7\,10^7$ s and hence the effect of the radiative deceleration is at most about 7000 km s^{-1}, which is small compared to 0.5 c.

The deceleration due to X-ray absorption can be estimated as follows. The power lost by the X-ray beam due to the absorption is about $4\,10^{36}$ W/sr. Therefore, the momentum lost per time interval per steradian is given by this number divided by c, or

$$dp/dt\,d\Omega = 1.3\,10^{28}\ \mathrm{N/sr}\,. \tag{32}$$

The absorbing cloud has a column density of $8\,10^{27}$ m^{-2} corresponding to 13 kg m^{-2}, or at the distance of 10^{14} m $1.3\,10^{29}$ kg/sr. Combining this with (35) we find a deceleration of 0.1 m s^{-2}, which again is too small to stop the cloud.

We conclude that a cloud similar to the broad line region clouds with a high velocity may reach a distance of $2\,10^{14}$ m from the central source without being decelerated significantly. But because the pressure balance with the confining medium is near the last stable point of the equilibrium curve (Krolik and Kallman, 1984) the cloud cannot come much closer to the central source; it will become unstable and will diffuse in the intercloud medium.

There are several uncertain factors in the quantitative estimates, however. The model calculations of Krolik and Kallman (1984) which we used in order to derive the absorption cross section of the hot cloud assumed a spectrum with photon index 2.0 between 1 eV and 400 keV. Clearly, in the hard X-ray regime the spectrum of III Zw 2 is much steeper (index 1.35) while it extends probably to at most 100 keV (see Sect. 4.1). Some differences in opacity caused by assuming different spectra may be found by comparing the just mentioned power law model of Krolik and Kallman and their model for a 2 keV thermal bremsstrahlung input spectrum. For the case of III Zw 2 (high ionisation of the cloud) the bremsstrahlung model gives a similar opacity as the power law model, however only for a cloud which has a much lower temperature: $2.5\,10^5$ K. The physical explanation for the different response of the cloud to different input spectra is that the number of ionising photons determines the ionisation degree, while their energy mainly determines the heating rate. The calculations of Krolik and Kallman (1984) are only valid when the optical thickness of the cloud is not too large. Our fit shows that this is not strictly the case for III Zw 2 at 2 keV, where the transmission is low (Fig. 6).

5. Conclusions

By comparing the observations obtained at different energies we have obtained knowledge about the physical conditions in III Zw 2. The most central part of the nucleus contains a black hole with a mass of $5\,10^7\,M_\odot$.The central engine is powered by an accretion flow of 2 solar masses per year, which cannot have lasted much longer than 20 million years. The accretion process is regulated by a massive accretion disk. Radiation pressure is the dominant pressure mechanism in the disk. In the inner parts of the disk, the radiation pressure is so large that the disk has an appreciable thickness: its maximum relative thickness is 0.8 and occurs at a distance of 10^{12} m from the black hole. Due to this thickness, we expect deviations from the ideal Shakura-Sunyaev disk equations to occur in the central part of the disk.

A very compact X-ray source with a radius of $3\,10^{11}$ m or 3 Schwarzschild radii is powered by the soft UV photons of the inner part of the disk. These soft photons are Compton-scattered and the result is a powerlaw spectrum with energy index -0.35 up to about 100 keV. The cut-off is caused by the relative low temperature of the X-ray source, about $2\,10^8$ K. The flare with a typical duration of one hour observed by Pounds (1986) can be explained by a burst of hard X-ray or gamma photons generated in the central parts of the X-ray source which diffuse through the central source by Compton scatterings. The X-ray radiation shows a moderate degree of beaming, due to the effective opening angle (50°) of the funnel of the accretion disk. Such a beaming is consistent with the observations of the optical line ratios.

The radiation of the most central 10^{13} m of the accretion disk is not observed directly as blackbody radiation, but is reprocessed. We argue that the energy generated in that part of the disk is converted in the synchrotron radiation observed as the infrared continuum powerlaw component. This component has a very large luminosity. The strong (10^{-3} T) magnetic field in this synchrotron source gives rise to the expectation that dynamo effects and magnetic pressure are important in the inner part of the accretion disk.

Somewhat further out in the accretion disk, at distances above 10^{13} m the optical/UV continuum is formed. The continuum flares which are observed at those wavelengths are proposed to be caused by instabilities in the outer part of the disk. The spectrum of the optical/UV continuum can be modeled simply by the sum of blackbody components which radiate the energy locally generated in the disk.

In the outer parts of the disk, at distances above $2\,10^{14}$ m self-gravity of the disk becomes important. This will result in deviations from the ideal Shakura-Sunyaev solution. It may also lead to instabilities which are visible in the inner parts of the disk (optical variations). From the observations of the optical line shapes, we deduced that the disk has a radius of about $9\,10^{15}$ m. The total disk mass is of the same order of magnitude as the mass of the central black hole.

Broad line region clouds are found at a distance $\sim 10^{16}$ m from the central black hole. The line profiles are explained by a model in which clouds emitting Balmer lines flow towards the central object with a typical velocity of 1200 km s^{-1} and a (one-dimensional) dispersion of 2000 km s^{-1}. Other clouds with a moderate optical depth emitting most of the Ly α and C IV flux flow outwards with a typical velocity of 1500 km s^{-1}. There is also a small number of clouds which reach very large velocities, visible up to 15000 km s^{-1} in the red wings of the Balmer lines. We investigated the possibility that the X-ray absorption feature described in Sec. 3 of this paper is such a high velocity cloud. If that interpretation is correct, the cloud must be close to the innermost radius where a two-phase equilibrium (Krolik et al., 1981) is possible ($2\,10^{14}$ m). This cloud has a typical density of 10^{16} m^{-3}, and a radius of $3\,10^{11}$ m. Its temperature of $9\,10^{5}$ K is so high because of the strong photo-ionisation heating by the X-ray continuum. The plasma in this cloud is nearly completely ionised, apart from a few heavy elements. A part of the incoming X-ray radiation is Compton scattered in the cloud into other directions, while especially near the ionisation edges of Mg, Si and S near 1 keV a part of the X-rays is absorbed. The cloud has a high velocity towards the central black hole of a considerable fraction of c. By extrapolating the observed red wing of the Balmer lines however, we expect indeed a few clouds to be present with velocities that high. Moreover, we showed that clouds with such velocities, when formed, cannot be decelerated sufficiently by the radiation pressure from the central X-ray source. Further X-ray observations with a better spectral resolution and higher sensitivity are needed to confirm the existence of similar clouds.

The strong synchrotron radio source in III Zw 2 is near the same region where the broad line region clouds are observed. We estimated a typical magnetic field of 10^{-5} T, and a typical size of $3\,10^{15}$ m at 10 GHz. This is just below the present capabilities of VLBI from Earth.

The optical line clouds are in pressure equilibrium with the hot, intercloud medium (Krolik et al., 1981). We have four distances to the central object in III Zw 2 where we can determine the intercloud gas pressure: in the X-ray source itself, from its inferred properties, near the hot absorbing cloud at $2\,10^{14}$ m and in the broad and narrow line region. It appears that the gas pressure from the central X-ray source up to the narrow line region (7 orders of magnitude in distance) is given within a factor of 2 by:

$$P_g \sim r^{-4/3}, \tag{33}$$

where the normalisation is 400 Pa at 10^{12} m. Since the temperature does not vary much from the central source ($2\,10^{8}$ K) to the narrow line region (probably $>10^{7}$ K), the density variation in the intercloud medium is very similar. If the X-ray radiation drives a strong stationary wind with a constant mass loss rate, then this density distribution leads to a decelerating flow, consistent with the observed narrow line profiles (Vrtilek, 1985).

Acknowledgement. The Laboratory for Space Research Leiden is supported financially by ZWO, The Netherlands Organisation for the Advancement of Pure Research.

References

Aller, H.D., Aller, M.F., Hodge, P.E.: 1981, *Astron. J.* **86**, 325

Andrew, B.H., MacLead, J.M., Harvey, G.A., Medd, W.J.: 1978, *Astron. J.* **83**, 863

Arp, H.: 1968, *Astrophys. J.* **152**, 1101

Balonek, T.J., Dent, W.A., Feldman, P.A., Andrew, B.H., MacLead, J.M.: 1979, *IAU Circ.* **3378**

Barr, P., Giommi, P., Wamsteker, W., Gilmozzi, R., Mushotzky, R.F.: 1985, *Bull. Am. Astron. Soc.* **17**, 608

Barr, P., Mushotzky, R.F.: 1986, *Nature* **320**, 421

Blandford, R.D.: 1985, in *Active Galactic Nuclei*, ed. J.E. Dyson, Manchester, U.K., p. 281

Boroson, T.A., Persson, S.E., Oke, J.B.: 1985, *Astrophys. J.* **293**, 120

De Bruyn, A.G., Sargent, W.L.W.: 1978, *Astron. J.* **83**, 1257

Carswell, R.F.: 1985, in *Active Galactic Nuclei*, ed. J.E. Dyson, Manchester, U.K., p. 157

Chapman, G.N.F., Geller, M.J., Huchra, J.P.: 1985, *Astrophys. J.* **297**, 151

Collin-Souffrin, S., Dumont, S., Joly, M., Péquignot, D.: 1986, *Astron. Astrophys.* **166**, 27

Collin-Souffrin, S.: 1987, *Astron. Astrophys.* **179**, 60

Condon, J.J., O'dell, S.L., Puschell, J.J., Stein, W.A.: 1981, *Astrophys. J.* **246**, 624

Edelson, R.A., Malkan, M.A.: 1986, *Astrophys. J.* **308**, 59

Elvis, M., Czerny, B., Wilkes, B.J.: 1986, Proc. ESA Workshop *The Physics of Accretion onto Compact Objects*, eds. K.O. Mason, M.G. Watson and N.E. White, Springer-Verlag

Fabian, A.C., Guilbert, P.W., Arnaud, K.A.: 1986, *Monthly Notices Roy. Astron. Soc.* **218**, 457

Felten, J.E., Rees, M.J.: 1972, *Astron. Astrophys.* **17**, 226

Gorenstein, P.: 1975, *Astrophys. J.* **198**, 95

Green, R.F.: 1976, *Publ. Astron. Soc. Pacific* **88**, 665

Green, R.F., Williams, T.B., Morton, D.C.: 1978, *Astrophys. J.* **226**, 729

Van Groningen, E.: 1983, *Astron. Astrophys.* **126**, 363

Hall, R., Ricketts, M.J., Page, C.G., Pounds, K.A.: 1981, *Space Sci. Rev.* **30**, 47

Heckman, T.M., Bothun, G.D., Balick, B., Smith, E.P.: 1984, *Astron. J.* **89**, 1958

Heiles, C.: 1975, *Astron. Astrophys. Suppl.* **20**, 37

Huchra, J., Geller, M., Morton, D.: 1981, *The Universe at Ultraviolet Wavelengths*, NASA Conf. Publ. 2171, p. 743

Huchtmeier, W.K., Wright, A.E.: 1973, *Astrophys. Letters* **15**, 209

Hutchings, J.B., Crampton, D., Campbell, B., Gower, A.C., Morris, S.C.: 1982, *Astrophys. J.* **262**, 48

Hutchings, J.B., Crampton, D., Campbell, B.: 1984, *Astrophys. J.* **280**, 41

Hutchings, J.B., Gower, A.C., Price, R.: 1987, *Astron. J.* **92**, 6

Kaastra, J.S., De Korte, P.A.J.: 1986 in Proc. Conf. *Variability of Galactic and Extragalactic X-ray Sources*, ed. A. Treves, Como, Italy, p. 47

Kellerman, K.I., Pauliny-Toth, I.I.K.: 1969, *Astrophys. J.* **155**, L71

Khachikian, E.Y., Weedman, D.W.: 1974, *Astrophys. J.* **192**, 581

De Korte, P.A.J., Bleeker, J.A.M., den Boggende, A.J.F., Branduari-Raymont, G., Brinkman, A.C., Culhane, J.L., Gronenschild, E.H.B.M., Mason, I., McKechnie, S.P.: 1981, *Space Sci. Rev.* **30**, 495
Krolik, J.H., McKee, C.F., Tarter, C.B.: 1981, *Astrophys. J.* **249**, 422
Krolik, J.H., Kallman, T.R.: 1984, *Astrophys. J.* **286**, 366
Kwan, J.: 1984, *Astropys. J.* **283**, 70
Landau, R., Epstein, E.E., Rather, J.D.G.: 1980, *Astron. J.* **85**, 363
Lawrence, A., Watson, M.G., Pounds, K.A., Elvis, M.: 1985, *Monthly Notices Roy. Astron. Soc.* **217**, 685
Lebofsky, M.J., Rieke, G.H.: 1980, *Nature* **284**, 410
Lloyd, C.: 1984, *Monthly Notices Roy. Astron. Soc.* **209**, 697
Malkan, M.A., Sargent, W.L.W.: 1982, *Astrophys. J.* **254**, 22
McAlary, C.W., McLaren, R.A., McGonegal, R.J., Maza, J.: 1983, *Astrophys. J. Suppl.* **52**, 341
Marshall, N., Warwick, R.S., Pounds, K.A.: 1981, *Monthly Notices Roy. Astron. Soc.* **194**, 987
Matilsky, T., Shrader, C., Tananbaum, H.: 1982, *Astrophys. J. Letters* **258**, L1
Morrison, R., McCammon, D.: 1983, *Astrophys. J.* **270**, 119
Neugebauer, G., Oke, J.B., Becklin, E.E., Matthews, K.: 1979, *Astrophys. J.* **230**, 79
Neugebauer, G., Miley, G.K., Soifer, B.T., Clegg, P.E.: 1986, *Astrophys. J.* **308**, 815
Osterbrock, D.E.: 1977, *Astrophys. J.* **215**, 733
Paczyński, B.: 1978, *Acta Astron.* **28**, 91
Peterson, C.G.B., Ferland, G.J.: 1986, *Nature* **324**, 345
Petre, R., Mushotzky, R.F., Krolik, J.H., Holt, S.S.: 1984, *Astrophys. J.* **280**, 499
Pica, A.J., Pollock, J.T., Smith, A.G., Leacock, R.J., Edwards, P.L., Scott, R.L.: 1980, *Astron. J.* **85**, 1442
Piccinotti, G., Mushotzky, R.F., Boldt, E.A., Holt, S.S., Marshall, F.E., Serlemitsos, P.J., Shafer, R.A.: 1982, *Astrophys. J.* **253**, 485
Pounds, K.A.: 1986, in Proc. Conf. *Variability of Galactic and Extragalactic X-ray Sources*, ed. A. Treves, Como, Italy, p. 1
Puetter, R.C., Smith, H.E., Willner, S.P., Pipher, J.L.: 1981, *Astrophys. J.* **243**, 345
Rieke, G.H., Lebofsky, M.J.: 1979, *Astrophys. J.* **227**, 710
de Robertis, M.: 1985, *Astrophys. J.* **289**, 67
Rudnick, L., Jones, T.W., Aller, H.D., Aller, M.F., Hodge, P.E., Owen, F.N., Fiedler, R.L., Puschell, J.J., Bignell, R.C.: 1985, *Astrophys. J. Suppl.* **57**, 693
Rybicky, G.B., Lightman, A.P.: 1979, *Radiative Processes in Astrophysics*, Wiley, New York
Sargent, W.L.W.: 1970, *Astrophys. J.* **160**, 405
Schillizzi, R.T.: 1976, *Astron. J.* **81**, 946
Schnopper, H.W., Delvaille, J.P., Epstein, A., Cash, W., Charles, P., Bowyer, S., Hjellming, R.M., Owen, F.N., Cotton, W.D.: 1978, *Astrophys. J.* **222**, L 91
Seaton, M.J.: 1979, *Monthly Notices Roy. Astron. Soc.* **187**, 73P
Shakura, N.I., Sunyaev, R.A.: 1973, *Astron. Astrophys.* **24**, 337
Shields, G.A.: 1978, Nature **272**, 706
Sikora, M.: 1981, *Monthly Notices Roy. Astron.* **196**, 257
Stasińska, G.: 1984, *Astron. Astrophys.* **135**, 341
Sunyaev, R.A., Titarchuk, L.G.: 1980, *Astron. Astrophys.* **86**, 121
Turner, M.J.L., Smith, A., Zimmerman, H.U.: 1981, *Space Sci. Rev.* **30**, 513
Unger, S.W., Lawrence, A., Wilson, A.S., Elvis, M., Wright, A.E.: 1987, *Monthly Notices Roy. Astron. Soc.* **228**, 521
Urry, C.M., Kruper, J.S., Canizares, C.R., Rohan, M.L., Oberhardt, M.R.: 1986, in Proc. Conf. *Variability of Galactic and Extragalactic x-ray Sources*, ed. A. Treves, Como, Italy, p. 15
Vrtilek, J.M.: 1985, *Astrophys. J.* **294**, 121
de Waard, G.J.: 1986, Thesis, Leiden
Wilkes, B.J.: 1986, *Monthly Notices Roy. Astron. Soc.* **218**, 331
Wittels, J.J., Cotton, W.D., Shapiro, I.I.: 1978, *Astrophys. J.* **225**, L47
Wright, A.E., Allen, D.A., Krug, P.A., Morton, D.C., Smith, M.G.: 1977, *IAU Circ.* 3145
Wu, C.C., Boggess, A., Gull, T.R.: 1983, *Astrophys. J.* **266**, 28
Zamorani, G., Giommi, P., Maccacaro, T., Tananbaun, H.: 1984, *Astrophys. J.* **278**, 28
Zwicky, F.: 1964, Lists of Compact Galaxies and Compact Parts of Galaxies
Zwicky, F.: 1967, *Adv. Astron. Astrophys.* **5**, 267